Geophysical Research Letters

RESEARCH LETTER
10.1029/2020GL088052

Key Points:
- Statistical maps of plasmaspheric hiss wave power and frequency, plasma density are provided based on Van Allen Probes 2012–2018 EMFISIS data
- MeV electron lifetimes decrease ~1.5–2 times during disturbed periods due to decreased ω_{pe}/Ω_{ce} as compared with statistical average values
- A MeV electron lifetime model (including hiss amplitude, frequency, ω_{pe}/Ω_{ce}) is presented and validated with the MagEIS electron lifetime database

Supporting Information:
- Supporting Information S1

Correspondence to:
O. Agapitov,
oleksiy.agapitov@gmail.com

Citation:
Agapitov, O., Mourenas, D., Artemyev, A., Claudepierre, S. G., Hospodarsky, G., & Bonnell, J. W. (2020). Lifetimes of relativistic electrons as determined from plasmaspheric hiss scattering rates statistics: Effects of ω_{pe}/Ω_{ce} and wave frequency dependence on geomagnetic activity. *Geophysical Research Letters*, *47*, e2020GL088052. https://doi.org/10.1029/2020GL088052

Received 20 MAR 2020
Accepted 21 MAY 2020
Accepted article online 30 MAY 2020

Lifetimes of Relativistic Electrons as Determined From Plasmaspheric Hiss Scattering Rates Statistics: Effects of ω_{pe}/Ω_{ce} and Wave Frequency Dependence on Geomagnetic Activity

O. Agapitov[1,2], D. Mourenas[3], A. Artemyev[4], S. G. Claudepierre[4,5], G. Hospodarsky[6], and J. W. Bonnell[1]

[1]Space Sciences Laboratory, University of California, Berkeley, CA, USA, [2]Astronomy and Space Physics Department, National Taras Shevchenko University of Kyiv, Kyiv, Ukraine, [3]CEA, DAM, DIF, Arpajon, France, [4]Department of Atmospheric and Oceanic Sciences, University of California, Los Angeles, CA, USA, [5]Space Sciences Department, The Aerospace Corporation, El Segundo, CA, USA, [6]Department of Physics and Astronomy, University of Iowa, Iowa City, IA, USA

Abstract Whistler-mode hiss waves generally determine MeV electron lifetimes inside the plasmasphere. We use Van Allen Probes measurements to provide the first comprehensive statistical survey of plasmaspheric hiss-driven quasi-linear pitch-angle diffusion rates and lifetimes of MeV electrons as a function of L^*, local time, and AE index, taking into account hiss power, electron plasma frequency to gyrofrequency ratio ω_{pe}/Ω_{ce}, hiss frequency at peak power ω_m, and cross correlations of these parameters. We find that during geomagnetically active periods with hiss observations, ω_{pe}/Ω_{ce} and ω_m decrease, leading to faster electron loss. We demonstrate that spatiotemporal variations of ω_m and ω_{pe}/Ω_{ce} with AE, together with wave power changes, significantly affect MeV electron loss, potentially leading to short lifetimes of less than 1 day. A parametric model of MeV electron lifetime driven by AE for $L > 2.5$ up to the plasmapause is developed and validated using Magnetic Electron Ion Spectrometer (MagEIS) electron flux decay database.

1. Introduction

Inside the plasmasphere, the lifetimes of megaelectron-volt (MeV) electrons in the outer radiation belt and in the slot region are known to be mostly determined by hiss wave-driven precipitation loss, as initially suggested by Lyons et al. (1972) and fully confirmed by recent works based on comparisons with accurate Van Allen Probes measurements of waves and electron lifetimes (Breneman et al., 2015; Ma et al., 2016; Mourenas et al., 2017; Ni et al., 2013; Pinto et al., 2019; Thorne et al., 2013). Hiss waves are intense (~10 – 100 pT) whistler-mode electromagnetic waves at ~50 – 2000 Hz excited inside the plasmasphere by anisotropic electrons during substorms and sometimes growing from a seed of chorus waves originating from outside the plasmasphere (Agapitov et al., 2018; Bortnik et al., 2011; Meredith et al., 2004; Su et al., 2018b). Plasmaspheric hiss amplitudes vary with L-shell, magnetic local time (MLT), and geomagnetic activity, with a major peak of hiss wave activity on the dayside (Agapitov et al., 2011, 2012, 2013, 2014; Green et al., 2005; Malaspina et al., 2016; Meredith et al., 2004; Spasojevic et al., 2015). The distribution of wave normal angles θ is predominantly field aligned in the vicinity of the geomagnetic equator, although θ is increasing nearly linearly with latitude λ (Artemyev et al., 2013; Agapitov et al., 2012, 2013; Horne et al., 2013). The variation of hiss amplitude with λ (up to 40°) is often weak (Agapitov et al., 2011, 2013; Artemyev et al., 2013; Spasojevic et al., 2015), indicating weak wave amplification/damping in the plasmasphere, so that equatorial amplitudes can be good estimates for hiss amplitudes up to $\lambda \approx 35 - 40°$. The best coverage of middle and high latitudes by the very-low-frequency (VLF) measurements was from Cluster (Agapitov et al., 2011, 2013), AKEBONO (Agapitov et al., 2014), and DE1 (Green et al., 2005) satellites, and these measurements mostly confirmed a weak dependence on λ, with the possible presence of an additional wave source at high latitude (above 45°). Recently, the evolution of plasmaspheric electron lifetimes with geomagnetic activity has been studied based on hiss power variations with AE or Kp obtained from the Van Allen Probes (Claudepierre et al., 2020; Mourenas et al., 2017; Orlova et al., 2016; Spasojevic et al., 2015), but the simultaneous spatiotemporal variations of the electron plasma frequency to gyrofrequency ratio ω_{pe}/Ω_{ce} and of

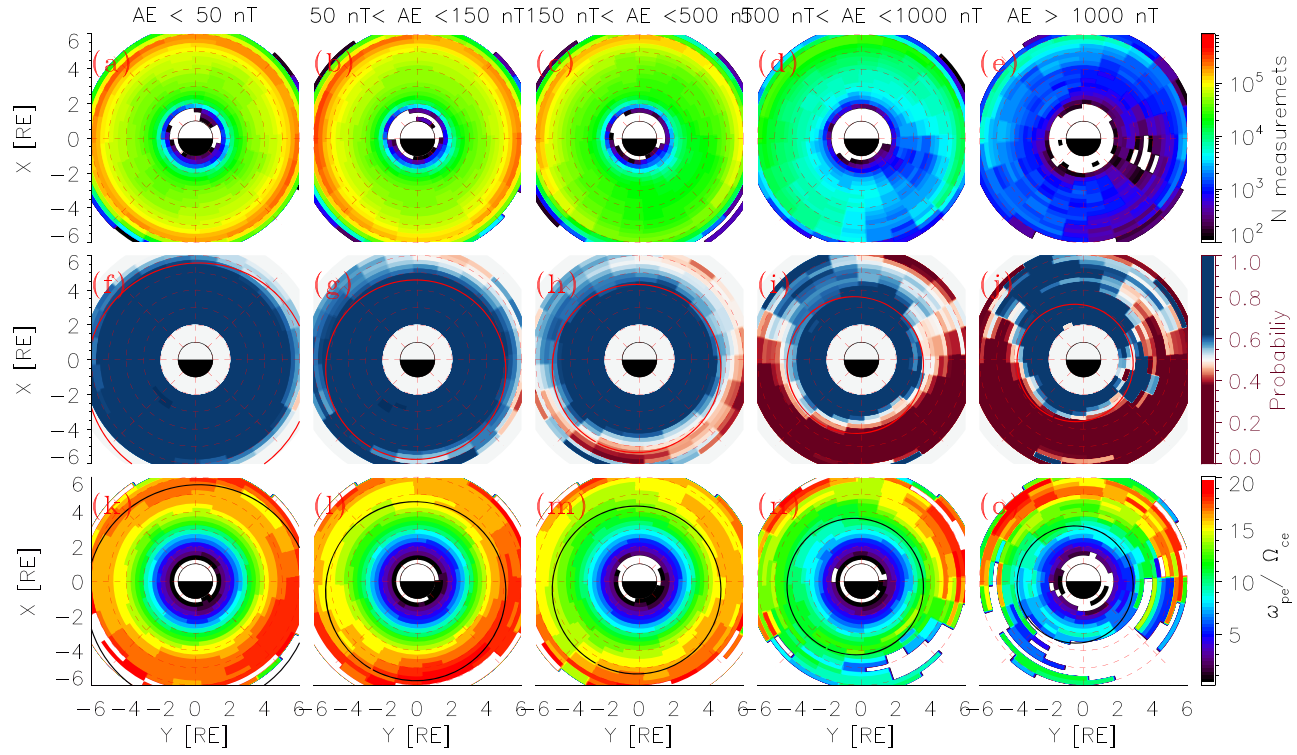

Figure 1. (a–e) Number of Van Allen Probes plasma density measurements available in each spatial bin and five *AE* ranges over 2012–2018. (f–j) Probability to be inside the plasmasphere based on the $N_e[cm^{-3}] > \max[15 \cdot (6.6/L)^4, 50]$ threshold. Red curves show the empirical plasmapause model from O'Brien and Moldwin (2003). (k–o) Distribution of the ω_{pe}/Ω_{ce} from EMFISIS HFR inside plasmasphere or plasmaspheric plumes, for different *AE* ranges.

the normalized hiss wave frequency still need to be taken into account to provide more accurate pitch-angle diffusion rates and electron lifetimes (Agapitov et al., 2019; Li et al., 2015; Lyons et al., 1972; Meredith et al., 2009; Mourenas et al., 2017; Mourenas & Ripoll, 2012; Summers et al., 2007).

To this end, we use VLF EMFISIS (The Electric and Magnetic Field Instrument Suite and Integrated Science) data (2012–2018) from the two Van Allen Probes spacecraft (Kletzing et al., 2013), considering geomagnetic activity level (*AE* index up to 1,200 nT), and binning VLF wave parameters and corresponding plasma parameters data (based on EMFISIS HFR measurements) to 0.1 R_E in *L*-shell and 1 hr in MLT (see satellite coverage in Figures 1a–1e and in Agapitov et al., 2019). We use plasma density N_e inferred from upper-hybrid resonance measurements (Kurth et al., 2015). Regions located inside the plasmasphere, or in plasmaspheric plumes, are defined here by a density $N_e[cm^{-3}] > \max[15 \cdot (6.6/L)^4, 50]$ (Figures 1f–1j), in agreement with the ω_{pe}/Ω_{ce} distribution inside and outside plasmasphere previously obtained by Agapitov et al. (2019) in the range *AE* ~ 0–1,200 nT. This density threshold is slightly higher than previously considered thresholds (Li et al., 2015; Sheeley et al., 2001), better excluding plasma trough or plasmapause transition regions where hiss is absent (Malaspina et al., 2016).

The statistical distribution of ω_{pe}/Ω_{ce} inside the plasmasphere is shown in Figures 1k–1o as a function of (*L*, MLT) for five *AE* ranges. A probability of 0.5 in Figures 1f–1j indicates the approximate location L_{pp} of the plasmapause, with an uncertainty similar to previous works (He et al., 2017; O'Brien & Moldwin, 2003). Although the limit of the plasmaspheric region is generally consistent with the plasmapause model $L_{pp}(AE)$ from O'Brien and Moldwin (2003) when *AE* < 500 nT, plasmaspheric plumes reach earlier MLT when *AE* > 500 nT and the nightside plasmasphere is then more eroded, like in test-particle simulations from Goldstein et al. (2014) during strong convection and plume formation. The global decrease of ω_{pe}/Ω_{ce} inside the plasmasphere by 20–30% from low to high *AE* in Figures 1k–1o is likely related to the simultaneous deeper erosion of the plasmasphere (Goldstein et al., 2014; O'Brien & Moldwin, 2003). This decrease of ω_{pe}/Ω_{ce} is expected to increase electron precipitation by plasmaspheric hiss for constant hiss power and frequency (Lyons et al., 1972; Mourenas et al., 2017). During extreme activity *AE* > 1,000 nT, a

high-density plume is found at L ~ 5–6, with an increased ω_{pe}/Ω_{ce}~20 around 8–10 MLT and 14–16 MLT where intense plume hiss generation and efficient electron loss may be expected (Li et al., 2019; Su et al., 2018a).

The distributions of plasmaspheric hiss wave power and frequency have already been studied based on limited data sets from the Van Allen Probes (Li et al., 2015; Meredith et al., 2018; Spasojevic et al., 2015; Yu et al., 2017). However, the effects of local hiss characteristics and plasma densities measured by the Van Allen Probes between 2012 and 2018 on the lifetimes of MeV electrons remain to be explored, in the same way as Meredith et al. (2009) and Summers et al. (2007) have estimated hiss and plasma density effects based on a single year of CRRES satellite data. This is the main purpose of the present work.

In the following, we provide the global statistics of MeV electrons lifetime as a function of (L^*, MLT, AE), based on comprehensive Van Allen Probes statistics of local hiss wave amplitude, frequency, and plasma density in 2012–2018 in the L^* range from 2.5 to the plasmapause, where electron dynamics are mostly determined by interactions with hiss waves. Adiabatically invariant L^*-shells are charged particles drift surfaces (usually close to L-shell values at low $L < 4$–4.5) and calculated here for high pitch-angle electrons (representing their main population) based on the Tsyganenko T89 magnetic field model using the Los Alamos National Laboratory library. For the first time, we consider the statistics of the electrons diffusion rates, taking into account simultaneously measured values of plasma density, wave frequency, and hiss wave power to more accurately quantify the statistical variations of such diffusion rates — that is, taking into account the correlations of wave and plasma parameters. Finally, parametrizations of 1-MeV electron lifetimes are presented and validated against recent estimates of electron lifetimes obtained from direct Magnetic Electron Ion Spectrometer (MagEIS) electron flux observations provided by Claudepierre et al. (2019, 2020).

2. 1-MeV Electron Hiss-Driven Diffusion Rates and Lifetimes: A Parametrization Taking Into Account the Effects of Variations of the Local ω_{pe}/Ω_{ce} Ratio and Hiss Frequency

The statistical distributions of hiss root-mean-square (RMS) amplitude B_w as a function of (L^*, MLT, AE) have already been provided based on 2-year (2012–2014) or 3-year (2012–2015) data sets from the Van Allen Probes (Meredith et al., 2018; Yu et al., 2017). We provide in Figures 2f–2j a more comprehensive statistics based on the full 6-year (2012–2018) Van Allen Probes data set, comprising in particular more numerous active periods (see Figures S1–S3 in supporting information). Moreover, we trace variations of other parameters of electron scattering models: hiss mean frequency and background plasma density. The local hiss mean frequency is obtained from the wave power distribution as $f_m = \omega_m / 2\pi = \sum_i \left(f_i * B_{wi}^2\right) / \sum_i \left(B_{wi}^2\right)$, giving a local f_m, a corresponding local wave power $B_w^2 = \sum_i \left(B_{wi}^2\right)$ for each wave spectrum, and a local ω_{pe}/Ω_{ce}, in each (L^*, MLT, AE, time) bin. A similar averaging procedure then gives the values of f_m, B_w^2, ω_{pe}/Ω_{ce} averaged over the full set of measurements in each (L^*, MLT, AE) bin under the form $g\left(L^*, \mathrm{MLT}, AE\right) = \sum_j \left(g_j B_{wj}^2\right) / \sum_j B_{wj}^2$ (j denoting counting in the set of measurements of each (L^*, MLT, AE) bin). This peculiar averaging procedure is more appropriate for wave effects processing than a simple average without weighting, because electron diffusion rates are proportional to wave power (see Appendix A) and, thus, periods of higher wave power have a stronger impact on electron scattering. The statistical distributions of average hiss wave power and mean frequency are displayed in Figures 2a–2j, revealing a decrease of hiss frequency as AE increases above 500 nT. The ω_{pe}/Ω_{ce} values simultaneously become ~20–30% smaller for $AE >$ 500 nT (Figures 1m–1o). Such smaller ω_m and ω_{pe}/Ω_{ce} correspond to a higher parallel energy for cyclotron-resonant anisotropic electrons generating these quasi-parallel hiss waves during higher AE periods (Kennel & Petschek, 1966; Mourenas et al., 2012). The correlation between ω_{pe}/Ω_{ce} and hiss wave amplitude B_w is very weak for $AE <$ 50 nT, but it increases to $R = 0.35 \pm 0.05$ for AE above 300 nT (see Figures S2–S4 in supporting information). In general, B_w increases with AE in the 5–19 MLT sector, although it nearly saturates above AE~500 nT at 4–11 MLT in Figures 2a–2e. Such an increase of hiss amplitude B_w with AE is probably due to stronger substorm-related injections of energetic electrons, with significantly larger temperature anisotropy during higher AE periods at the energy of cyclotron resonance with hiss waves (e.g., Liu et al., 2020). It could also be due to a partial seeding of hiss waves by

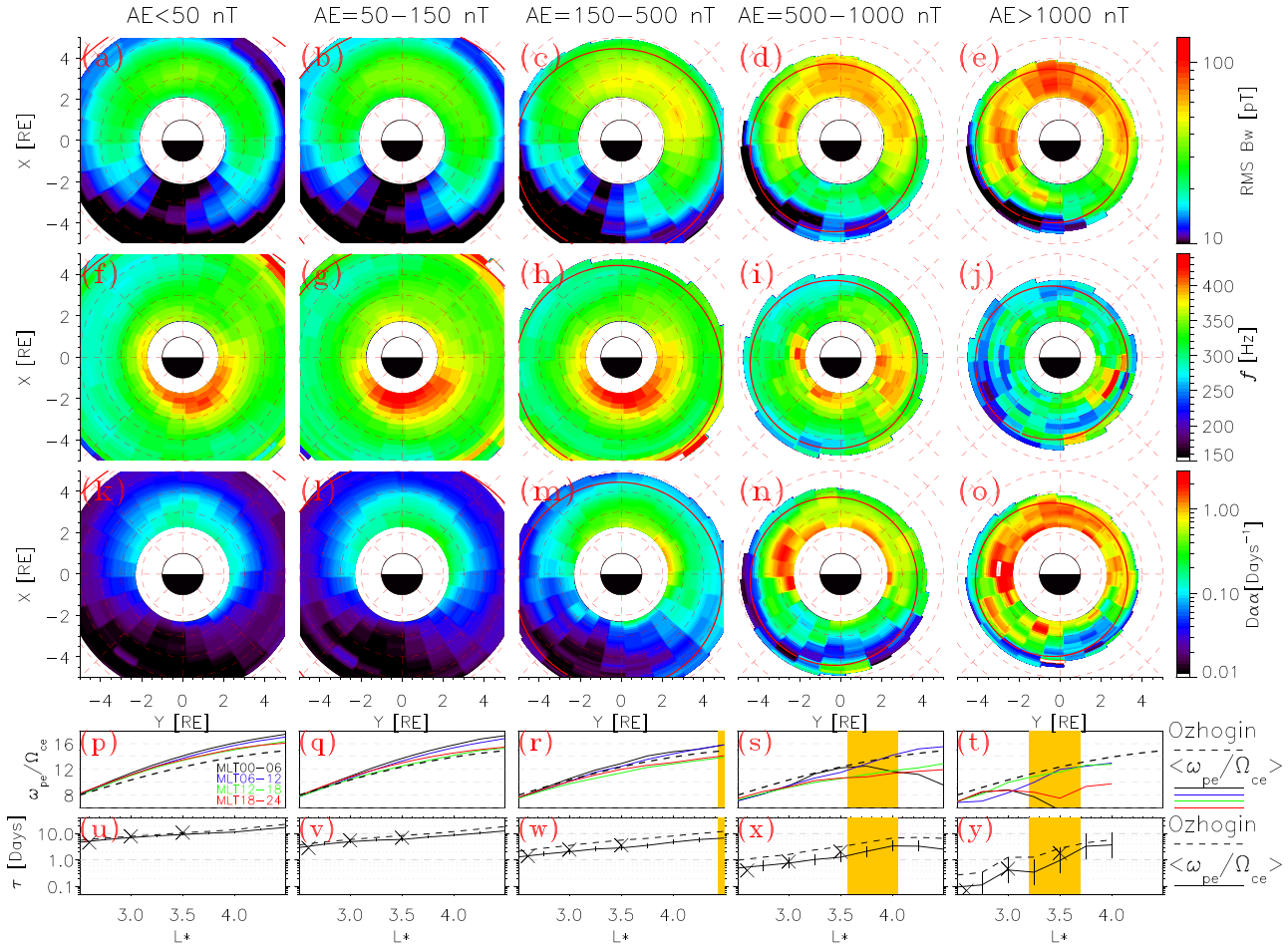

Figure 2. (a–e) Distribution of hiss RMS amplitude B_w from EMFISIS HFR in the plasmasphere or in plumes, for the same geomagnetic activity levels as in Figure 1. The outer limit of the region of plasmaspheric hiss waves determined by the plasmapause model of O'Brien and Moldwin (2003) is shown by solid red curves. (f–j) Distribution of hiss wave frequency at peak wave amplitude as a function of *AE*. (k–o) Distribution of corresponding bounce-averaged pitch-angle diffusion rates. (p–t) Distributions of ω_{pe}/Ω_{ce} in four MLT sectors (00–06, 06–12, 12–18, and 18–24 MLT indicated by black, blue, green, and red colors, respectively), and ω_{pe}/Ω_{ce} obtained making use of a statistical plasma density model (Ozhogin et al., 2012). (u–y) 1-MeV electrons lifetimes obtained from analytical estimates (solid curves) or from full numerical calculations (crosses) making use of Van Allen Probes data of ω_{pe}/Ω_{ce} and ω/Ω_{ce}, or calculated using the statistical plasma density model (dashed curves).

incoming chorus waves, whose power is known to strongly increase with *AE* (Agapitov et al., 2017, 2018, 2019; Bortnik et al., 2011), and to a more efficient reflection and focusing of hiss waves near the shrinking plasmapause (Su et al., 2018a).

It is already known that a smaller ω_{pe}/Ω_{ce} leads to faster hiss-driven electron precipitation loss (Agapitov et al., 2019; Artemyev et al., 2013; Lyons et al., 1972; Mourenas et al., 2017; Mourenas & Ripoll, 2012; Summers et al., 2007) and that ω_{pe}/Ω_{ce} can be reduced inside the plasmasphere during strong disturbances seen in Figures 1k–1o and in Agapitov et al. (2019). The dependence of ω_{pe}/Ω_{ce} on L^* in the four MLT sectors is presented in Figures 2p–2t, showing a significant decrease of ω_{pe}/Ω_{ce} from quiet to disturbed geomagnetic conditions, especially for $AE > 500$ nT, leading to smaller values during disturbed periods than in the statistical average plasma density model from Ozhogin et al. (2012). Hereafter, we consider approximate analytical estimates of the pitch-angle diffusion rate $D_{\alpha\alpha}$ of electrons by hiss waves, provided in Appendix A (and derived using the method described in Artemyev et al., 2013; Mourenas & Ripoll, 2012), which have been extensively validated against both numerical simulations and observations (Artemyev et al., 2013; Mourenas et al., 2016, 2017; Mourenas & Ripoll, 2012; Pinto et al., 2019). Using such simplified analytical expressions allows a tremendous acceleration of numerical calculations of *local* (in space and time) bounce-averaged diffusion rates $D_{\alpha\alpha}$ in all (L^*, MLT, *AE*) bins, based on all measured

local (in space and time) plasma and wave parameters. This allows us, for the first time, to fully include the effects of local plasma conditions, hiss wave frequency and power, and of their cross correlations, on the scattering and lifetimes of 1-MeV electrons as a function of L^*, MLT, and AE in the plasmasphere, complementing previous works that included only an increase of hiss power with AE (Meredith et al., 2004; Spasojevic et al., 2015). This is done automatically through the calculation of local bounce-averaged scattering rates $D_{\alpha\alpha}$ for each set of local satellite measurements, providing us with diffusion coefficients $D_{\alpha\alpha}$ statistics that are then averaged over time and used to construct statistics of relativistic electrons lifetimes. At sufficiently high $L^* > 2.5$–2.7 in the plasmasphere, the lifetime τ of 1-MeV electrons is indeed controlled by pitch-angle diffusion near the loss-cone angle α_{LC} (Albert, 2005; Albert & Shprits, 2009; Artemyev et al., 2013; Mourenas et al., 2012), and it can be written under a simple form:

$$\tau[\text{days}] \approx \ln|\sin(\pi/4)/\sin\alpha_{LC}|/\left(4\langle D_{\alpha\alpha}\rangle_{MLT}\right), \quad (1)$$

using the analytical $D_{\alpha\alpha}$ averaged over MLT and $\sin\alpha_{LC} = 1/(L^{*3/2}[4 - 3/L^*]^{1/4})$ (Artemyev et al., 2013; Mourenas & Ripoll, 2012). This analytical estimate generally remains within a factor ~1.5–2 of exact numerical solutions (Figures 2u–2y show the actual agreement between analytical estimates and full numerical calculations) and of measured lifetimes over a wide range of L^* and energies E, provided that $E_0 < E <$ 3–4 MeV and $L^* <$ 4.0–4.5—so that the effects of Landau resonance (at low E) and electromagnetic ion cyclotron (EMIC) waves (at high E and L^*) remain limited when considering usual electron flux decays over days to weeks (Artemyev et al., 2013; Mourenas et al., 2016, 2017; Mourenas & Ripoll, 2012; Pinto et al., 2019; Zhang et al., 2016). Here, E_0 corresponds to the minimum electron energy such that cyclotron resonance is available with hiss waves at all frequencies $f > f_m/2$ ($E_0 \sim$ 0.7–1 MeV for L^*~2.6 and $E_0 <$ 1 MeV at higher L^*—e.g., see Mourenas et al., 2012, 2017), as assumed in the analytical model. Based on the observed ω_{pe}/Ω_{ce} levels, the condition $E > E_0$ approximately corresponds to a condition $L^* > 2.5 - 2.6$ for $E \sim E_0 \sim$ 1 MeV electrons for the applicability of this analytical lifetime model.

Maps of the obtained diffusion rates $D_{\alpha\alpha}$ are provided in Figures 2k–2o. Strong diffusion rates, only found in the day sector for low $AE <$ 50 nT, progressively extend to the ~5–19 MLT sector as AE increases. The L^* of maximum scattering simultaneously increases from ~2 to ~3 as AE increases, getting closer to the lowered plasmapause during periods of very high $AE >$ 1,000 nT, such that the statistical $D_{\alpha\alpha}$ locally reaches >1/day. As geomagnetic activity increases, 1-MeV electron lifetimes $\tau_{1\ MeV}$ at $2.5 < L^* < 5$ in Figures 2u–2y and 3a progressively decrease from ~5–20 days during quiet periods ($AE =$ 50–150 nT) down to ~0.25–1 day during active periods ($AE >$ 500 nT). The decrease of ω_{pe}/Ω_{ce} and ω_m/Ω_{ce} as AE increases above 800 nT leads to a ~1.5–2 times decrease of 1-MeV electron lifetimes in Figures 2u–2y as compared with values obtained using a statistical plasma density model (Ozhogin et al., 2012). Such lifetimes are in good agreement with the actual lifetimes derived from Van Allen Probes particle measurements at $L^* = 2.5 - 5$ during active periods with $K_p = 2$ (Mourenas et al., 2017) as well as with their statistical range of variation (Claudepierre et al., 2020).

During quiet times ($AE <$ 150 nT), taking into account measured local plasma density variations gives similar lifetimes as for a statistical model of average plasmaspheric density (Ozhogin et al., 2012). For $AE >$ 150–500 nT, however, local plasma density variations have a significant effect on hiss-driven electron diffusion, generally reducing 1-MeV electron lifetimes by a factor ~1.5–2.0 (see Figures 2u–2y). Indeed, ω_{pe}/Ω_{ce} decreases during active periods in nearly all MLT sectors, leading to significantly faster electron precipitation into the atmosphere. An additional factor amplifying precipitation rates is the decrease of the normalized hiss mean frequency by 10–20% for $AE >$ 800 nT.

The dependence of 1-MeV electron lifetimes on L^* and AE found in Figure 3a can be well parameterized by a two-dimensional polynomial of third order:

$$\log(\tau_{1\ MeV}) = a_{ij} AE^i L^{*j} * F\left(AE, L^*\right), \quad (2)$$

where coefficients a_{ij} (provided in Table 1) are derived from the distribution shown in Figure 3a by least square minimization of the residuals, with a correction factor $F(AE, L^*)$ provided to take into account the

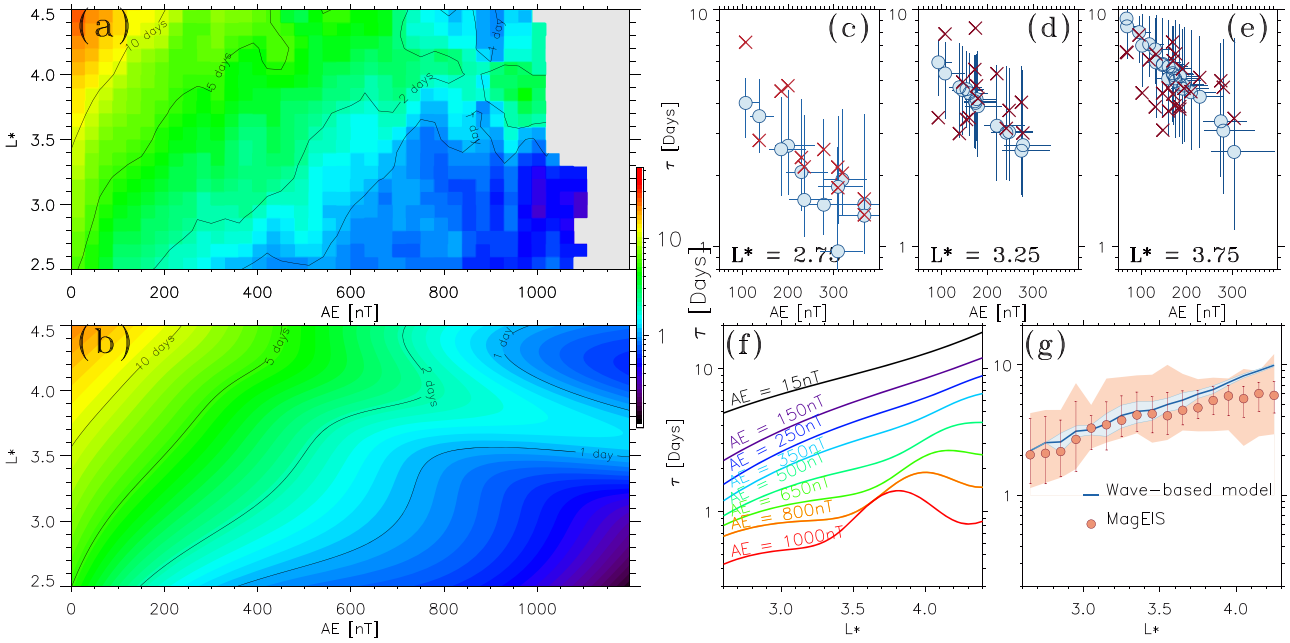

Figure 3. (a) 1-MeV electron lifetime $\tau_{1\ \mathrm{MeV}}$ in the L^* and *AE*-index domain, calculated from $D_{\alpha\alpha}$ distributions (in Figures 2k–2o) obtained from Van Allen Probes measurements. (b) Corresponding $\tau_{1\ \mathrm{MeV}}$ parametrization based on Equation (2) and Table 1. (c, d) Comparison of $\tau_{1\ \mathrm{MeV}}$ from the model (blue circles) with direct estimations (red crosses) from Claudepierre et al. (2020) based on Van Allen Probes MagEIS measurements of electron flux at $L^* = 2.75$, 3.25, and 3.75, respectively. (f) The model values of $\tau_{1\ \mathrm{MeV}}$ for different levels of geomagnetic activity (*AE* from 0 to 1,000 nT, indicated by curves colors). (g) Averaged measured lifetime of 1-MeV electrons obtained by Claudepierre et al. (2020) (red circles showing the mean, bars showing two standard deviations, and red zone showing the full variation) and model of $\tau_{1\ \mathrm{MeV}}$ (blue curve).

increase of $\tau_{1\ \mathrm{MeV}}$ in the vicinity of the statistical plasmapause position, which generally comes closer to the Earth when *AE* (in nT) increases (O'Brien & Moldwin, 2003):

$$F(AE, L^*) = 1 + \exp\left(-9.7 \cdot \left(L^* - 4.6 + AE/1,251\right)^2\right) \cdot (AE/830)^2. \quad (3)$$

The corresponding model $\tau_{1\ \mathrm{MeV}}$ mapping shown in Figure 3b reproduces well the observed variations of 1-MeV electron lifetimes with L^* and *AE*. Note that hiss measurements in the plasmasphere are more infrequent and less uniformly distributed in MLT at high $L^* > 3.5$–4.0 when $AE > 800$–900 nT, corresponding to less reliable lifetime estimates. Claudepierre et al. (2019, 2020) have provided estimates of electron decay rates obtained based on Van Allen Probes MagEIS measurements of electron fluxes in 2014–2018 (available in the supporting information of their papers). We processed geomagnetic activity during the intervals of this database of decay rates and calculated the model $\tau_{1\ \mathrm{MeV}}(L^*, AE)$ for each interval (representing 5 to 30 intervals for each L^*). Such model lifetime values are shown in Figures 3c–3e together with measured lifetime values from Claudepierre et al. (2020) at $L^* = 2.75$ to 3.75. As demonstrated by Figures 3c–3e, the lifetime model $\tau_{1\ \mathrm{MeV}}$ reproduces well, both qualitatively and quantitatively, the increase of measured lifetimes with L^* and their decrease as *AE* increases (especially when taking into account the uncertainty of the model $\tau_{1\ \mathrm{MeV}}$ corresponding to the variation of *AE* during the considered

Table 1
The Coefficients a_{ij} of Model 1-MeV Electron Lifetimes Given by Equation (2)

a_{ij}	i			
j	2.04 ± 0.17	$(1.02 \pm 0.2)\cdot 10^{-2}$	$(8.08 \pm 1.1)\cdot 10^{-6}$	$(4.69 \pm 1.2)\cdot 10^{-9}$
	2.19 ± 0.16	$(1.96 \pm 0.2)\cdot 10^{-2}$	$(7.24 \pm 1.7)\cdot 10^{-6}$	$(-3.79 \pm 1.0)\cdot 10^{-9}$
	$(-5.84 \pm 0.51)^{-1}$	$(7.12 \pm 1.1)\cdot 10^{-2}$	$(-5.13 \pm 1.7)\cdot 10^{-6}$	$(2.78 \pm 1.2)\cdot 10^{-9}$
	$(5.86 \pm 0.58)^{-2}$	$(-1.58 \pm 0.2)\cdot 10^{-4}$	$(6.90 \pm 2.1)\cdot 10^{-7}$	$(-3.73 \pm 1.3)\cdot 10^{-10}$

decay intervals). The model $\tau_{1\ \mathrm{MeV}}(L^*, AE)$ variations are also displayed in Figure 3f. Model lifetimes $\tau_{1\ \mathrm{MeV}}$ in Figure 3g are also in very good agreement with the average measured lifetimes from Claudepierre et al. (2020) plotted as a function of $L^* = 2.5$ to 3.8 (at higher L^*, particle drift trajectories come partially outside the plasmasphere and can be affected by chorus waves). For $E_0 < E < 4$ MeV, electron lifetimes increase with energy like (Mourenas & Ripoll, 2012; Pinto et al., 2019):

$$\tau(E)/\tau_{1\ \mathrm{MeV}} \approx 0.194 \cdot (1 + 2E)\left(E^2 + E\right)^{7/9}, \tag{4}$$

where E is in MeV. Therefore, the lifetimes of electrons in this energy range can be deduced from model lifetimes $\tau_{1\ \mathrm{MeV}}$ from Equation (2), validated against the database from Claudepierre et al. (2020), providing an estimation of the contribution of hiss waves to the precipitation of 1–4 MeV electrons. However, above ~2–3 MeV and for $L^* > 4$–4.5 inside the plasmasphere, the contribution of EMIC waves to electron diffusion may have to be taken into account to estimate full scattering rates and decay rates within the plasmasphere (Mourenas et al., 2016, 2017; Pinto et al., 2019; Zhang et al., 2016).

Finally, let us emphasize that both estimated and measured lifetimes of 1-MeV electrons are generally larger than ~3 to 20 days from $L^* = 3$ to $L^* = 5$ (Mourenas et al., 2017). This justifies using, in each (L^*, AE) bin, wave and plasma data averaged over the corresponding total integrated time of measurements of ~30 days (in the day sector) provided by 6-year Van Allen Probes statistics, even if the $D_{\alpha\alpha}$ distribution is non-Gaussian (Watt et al., 2019). Indeed, we checked that the MLT-averaged $D_{\alpha\alpha}$ obtained from Van Allen Probes data in a given (L^*, AE) bin does remain similar from year to year over smaller integrated periods of measurements of ~4–10 days (see Figure S1 in supporting information).

3. Conclusions

Making use of the full 2012–2018 Van Allen Probes data set, we have provided comprehensive statistical maps of plasmaspheric hiss-driven pitch-angle diffusion rates of MeV electrons as a function of L^*, MLT, and AE, which take into account the local hiss wave power, the dynamics of the electron plasma frequency to gyrofrequency ratio ω_{pe}/Ω_{ce}, and hiss frequency f_m at peak wave power, but also the spatiotemporal correlations between these parameters. Statistics of MeV electron lifetimes have been provided and analyzed. We found that during active periods with $AE > 150$ nT, ω_{pe}/Ω_{ce} and f_m decrease in nearly all MLT sectors, leading to faster electron precipitation into the atmosphere. The spatiotemporal variations of ω_{pe}/Ω_{ce} with AE, together with wave power and frequency changes, strongly affect 1-MeV electron lifetimes, potentially leading near $L^* = 2.6$ to very short lifetimes of less than ~1 day during active periods with $AE > 500$ nT (down to ~6 hr for $AE > 1{,}000$ nT), and explaining the observations reported in Claudepierre et al. (2020) and Mourenas et al. (2017) without requiring additional electromagnetic ion cyclotron (EMIC) waves to reach such small lifetimes (Mourenas et al., 2016). This effect alone can explain the general absence of strong fluxes of MeV electrons at $L^* < 2.8$ (Baker et al., 2014), although Ozeke et al. (2018) have shown that the finite duration of strong solar wind driving during a single storm may similarly limit the inward radial diffusion of MeV electrons driven by ULF waves.

A parameterization of MeV electrons lifetimes due to hiss-driven pitch-angle scattering has been developed, valid for $AE = 0$ up to 1,100–1,200 nT at $2.6 < L^* < 3.5$ and up to 900–1,000 nT at $L^* = 3.5$–4.5 inside the plasmasphere. The plasma- and wave-based lifetimes are in good agreement with recent measured electron lifetimes from the Van Allen Probes (Claudepierre et al., 2020) in the region of efficient electron scattering by hiss waves (from $L^* \sim 2.6$ up to the plasmapause) between $L^* = 2.6$ and $L^* = 3.9$ for $AE = 0$ up to 400 nT at least. Therefore, this recalculated lifetime model can explain the behavior of 1-MeV electrons in the L^* range from 2.6 to ~3.9, and it can be used as a realistic estimation of hiss contribution to electron precipitation rates above $L^* = 3.8$ or at higher electron energies, where the contributions from EMIC and chorus waves may become significant.

Data Availability Statement

Van Allen Probe EMFISIS data are available at the website (http://emfisis.physics.uiowa.edu/data/index). We acknowledge W. S. Kurth for providing plasma density estimations. EFW data are available at the website (http://www.space.umn.edu/rbspefw-data/).

Appendix A

The diffusion coefficient $D_{\alpha\alpha}$ for electron scattering by whistler-mode waves in inhomogeneous plasma includes averaging (integration) over wave frequency range, wave normal angle θ distribution, and electron bounce period. These integrations can be simplified for reasonable assumptions about the small ratio of wave mean frequency to electron gyrofrequency ω_m/Ω_{ce} (well established for hiss waves with $\omega_m/\Omega_{ce} < 0.1$), sufficiently narrow distributions of wave frequency $\Delta\omega/\omega_m < 1$ and wave normal angles $\theta < 50$–$60°$, and a short range of resonance latitudes $\Delta\lambda_R$ (see details in Mourenas et al., 2012; Mourenas & Ripoll, 2012). This range for a nearly dipolar magnetic field model is determined by the width of the frequency distribution, $\Delta\omega$, whereas the resonance latitude λ_R is determined by the wave mean frequency ω_m for first cyclotron resonance (the most important for quasi-parallel wave propagation) and $\Delta\lambda_R$ is equal to $\min(\lambda_{\max}, \lambda_{R+}) - \lambda_{R-}$, with $\lambda_{R\pm} = \lambda_R \pm \left[\left(\lambda_R^2 + \frac{2\Delta\omega}{27\omega_m(p\varepsilon_m)^{1/9}}\right)^{1/2} - \lambda_R\right]$, and $\varepsilon_m = \frac{\omega_{pe}}{\Omega_{ce}}\sqrt{\frac{\omega_m}{\Omega_{ce}}}$. $\lambda_{\max} \approx 35°$ is the maximum latitude of strong hiss wave presence, $p = (\gamma^2 - 1)^{1/2}$, γ is the relativistic factor. Using this definition of $\Delta\lambda_R$, one can estimate the diffusion rate $D_{\alpha\alpha}$ as in (Artemyev et al., 2013):

$$D_{\alpha\alpha} \approx \frac{\pi B_w^2}{4B_0^2 T_b \cos^2\alpha_{LC}} \frac{\Omega_{ce}\omega_m}{\Delta\omega} \frac{\Delta\lambda_R\left(1 + 3\sin^2\lambda_R\right)^{7/12}}{\varepsilon_m^{13/9}\gamma(\gamma^2-1)^{13/18}} \frac{(1 - \omega_m/\Omega_{ce}) \quad |1 - \gamma\omega_m/\Omega_{ce}|^{-4/9}}{|\gamma(\omega_m/\Omega_{ce}) - 2\gamma(\omega_m/\Omega_{ce})^2 + 1|},$$

where $T_b \approx 1.38 - 0.64\sin^{3/4}\alpha_{LC}$. Note that all terms in the equations are evaluated at the equatorial plane. For more details, see Artemyev et al. (2013), where this approximation has been validated for a wide range of wave parameters corresponding to quiet, intermediate, and disturbed regimes of geomagnetic activity.

Acknowledgments

The work of O. A. and A. A. was supported by National Aeronautics and Space Administration (NASA) LWS Grant 80NSSC20K0218 and NSF grant number 1914670. The work of O. A. was partially supported by NASA Grants 80NNSC19K0848 and 80NSSC19K0264.

References

Agapitov, O., Artemyev, A., Krasnoselskikh, V., Khotyaintsev, Y. V., Mourenas, D., Breuillard, H., et al. (2013). Statistics of whistler mode waves in the outer radiation belt: Cluster STAFF-SA measurements. *Journal of Geophysical Research: Space Physics*, *118*(6), 3407-3420. https://doi.org/10.1002/jgra.50312

Agapitov, O., Artemyev, A., Mourenas, D., Kasahara, Y., & Krasnoselskikh, V. (2014). Inner belt and slot region electron lifetimes and energization rates based on AKEBONO statistics of whistler waves. *Journal of Geophysical Research: Space Physics*, *119*, 2876–2893. https://doi.org/10.1002/2014JA019886

Agapitov, O., Krasnoselskikh, V., Khotyaintsev, Y. V., & Rolland, G. (2011). A statistical study of the propagation characteristics of whistler waves observed by Cluster. *Geophysical Research Letters*, *38*, L20103. https://doi.org/10.1029/2011GL049597

Agapitov, O., Krasnoselskikh, V., Khotyaintsev, Y. V., & Rolland, G. (2012). Correction to "A statistical study of the propagation characteristics of whistler waves observed by Cluster". *Geophysical Research Letters*, *39*, L24102. https://doi.org/10.1029/2012GL054320

Agapitov, O., Mourenas, D., Artemyev, A., Hospodarsky, G., & Bonnell, J. W. (2019). Time scales for electron quasi-linear diffusion by lower-band chorus waves: The effects of ωpe/Ωce dependence on geomagnetic activity. *Geophysical Research Letters*, *46*, 6178–6187. https://doi.org/10.1029/2019GL083446

Agapitov, O., Mourenas, D., Artemyev, A., Mozer, F. S., Bonnell, J. W., Angelopoulos, V., et al. (2018). Spatial extent and temporal correlation of chorus and hiss: Statistical results from multipoint THEMIS observations. *Journal of Geophysical Research: Space Physics*, *123*, 8317–8330. https://doi.org/10.1029/2018JA025725

Agapitov, O. V., Mourenas, D., Artemyev, A. V., Mozer, F. S., Hospodarsky, G., Bonnell, J., & Krasnoselskikh, V. (2017). Synthetic empirical chorus wave model from combined Van Allen probes and cluster statistics. *Journal of Geophysical Research: Space Physics*, *123*, 297–314. https://doi.org/10.1002/2017JA024843

Albert, J. M. (2005). Evaluations of quasi-linear diffusion coefficients for whistler mode waves in a plasma with arbitrary density ratio. *Journal of Geophysical Research*, *110*, A03218. https://doi.org/10.1029/2004JA010844

Albert, J. M., & Shprits, Y. Y. (2009). Estimates of lifetimes against pitch angle diffusion. *Journal of Atmospheric and Solar - Terrestrial Physics*, *71*(16), 1647–1652. https://doi.org/10.1016/j.jastp.2008.07.004

Artemyev, A., Mourenas, D., Agapitov, O., & Krasnoselskikh, V. (2013). Parametric validations of analytical lifetime estimates for radiation belt electron diffusion by whistler waves. *Annales Geophysicae*, *31*(4), 599–624. https://doi.org/10.5194/angeo-31-599-2013

Baker, D. N., Jaynes, A. N., Hoxie, V. C., Thorne, R. M., Foster, J. C., Li, X., et al. (2014). An impenetrable barrier to ultrarelativistic electrons in the Van Allen radiation belts. *Nature*, *515*(7528), 531–534. https://doi.org/10.1038/nature13956

Bortnik, J., Chen, L., Li, W., Thorne, R. M., & Horne, R. B. (2011). Modeling the evolution of chorus waves into plasmaspheric hiss. *Journal of Geophysical Research*, *116*, A08221. https://doi.org/10.1029/2011JA016499

Breneman, A. W., Halford, A., Millan, R., McCarthy, M., Fennell, J., Sample, J., et al. (2015). Global-scale coherence modulation of radiation-belt electron loss from plasmaspheric hiss. *Nature*, *523*(7559), 193–195. https://doi.org/10.1038/nature14515

Claudepierre, S. G., Ma, Q., Bortnik, J., O'Brien, T. P., Fennell, J. F., & Blake, J. B. (2020). Empirically estimated electron lifetimes in the Earth's radiation belts: 2. Comparison with theory. *Geophysical Research Letters*, *47*, e2019GL086056. https://doi.org/10.1029/2019GL086056

Claudepierre, S. G., O'Brien, T. P., Looper, M. D., Blake, J. B., Fennell, J. F., Roeder, J. L., et al. (2019). A revised look at relativistic electrons in the Earth's inner radiation zone and slot region. *Journal of Geophysical Research: Space Physics*, *124*, 934–951. https://doi.org/10.1029/2018JA026349

Goldstein, J., De Pascuale, S., Kletzing, C., Kurth, W., Genestreti, K. J., Skoug, R. M., et al. (2014). Three-dimensional electron radiation belt simulations using the BAS Radiation Belt model with new diffusion models for chorus, plasmaspheric hiss, and lightning-generated whistlers. *Journal of Geophysical Research: Space Physics*, *119*, 268–289. https://doi.org/10.1002/2013JA019281

He, F., Zhang, X.-X., Lin, R.-L., Fok, M.-C., Katus, R. M., Liemohn, M. W., et al. (2017). A new solar wind-driven global dynamic plasmapause model: 2. Model and validation. *Journal of Geophysical Research: Space Physics*, *122*, 7172–7187. https://doi.org/10.1002/2017JA023913

Horne, R. B., Kersten, T., Glauert, S. A., Meredith, N. P., Boscher, D., Sicard-Piet, A., et al. (2013). A new diffusion matrix for whistler mode chorus waves. *Journal of Geophysical Research: Space Physics*, *118*, 6302–6318. https://doi.org/10.1002/jgra.50594

Green, J. L., Boardsen, S., Garcia, L., Taylor, W. W. L., Fung, S. F., & Reinisch, B. W. (2005). On the origin of whistler mode radiation in the plasmasphere. *Journal of Geophysical Research: Space Physics*, *110*(A9), 3201. https://doi.org/10.1029/2004JA010495

Kennel, C. F., & Petschek, H. E. (1966). Limit on stably trapped particle fluxes. *Journal of Geophysical Research*, *71*(1), 1–28. https://doi.org/10.1029/JZ071i001p00001

Kletzing, C. A., Kurth, W. S., Acuna, M., MacDowall, R. J., Torbert, R. B., Averkamp, T., et al. (2013). The electric and magnetic field instrument suite and integrated science (EMFISIS) on RBSP. *Space Science Reviews*, *179*, 127–181. https://doi.org/10.1007/s11214-013-9993-6

Kurth, W. S., De Pascuale, S., Faden, J. B., Kletzing, C. A., Hospodarsky, G. B., Thaller, S., & Wygant, J. R. (2015). Electron densities inferred from plasma wave spectra obtained by the waves instrument on Van Allen probes. *Journal of Geophysical Research: Space Physics*, *120*, 904–914. https://doi.org/10.1002/2014JA020857

Li, W., Shen, X. C., Ma, Q., Capannolo, L., Shi, R., Redmon, R. J., et al. (2019). Quantification of energetic Electron precipitation driven by plume whistler mode waves, Plasmaspheric hiss, and exohiss. *Geophysical Research Letters*, *46*, 3615–3624. https://doi.org/10.1029/2019GL082095

Liu, N., Su, Z., Gao, Z., Zheng, H., Wang, Y., Wang, S., et al. (2020). Comprehensive observations of substorm-enhanced plasmaspheric hiss generation, propagation, and dissipation. *Geophysical Research Letters*, *47*(2), e2019GL086040. https://doi.org/10.1029/2019GL086040

Lyons, L. R., Thorne, R. M., & Kennel, C. F. (1972). Pitch-angle diffusion of radiation belt electrons within the plasmasphere. *Journal of Geophysical Research*, *77*(19), 3455–3474. https://doi.org/10.1029/JA077i019p03455

Li, W., Ma, Q., Thorne, R. M., Bortnik, J., Kletzing, C. A., Kurth, W. S., et al. (2015). Statistical properties of plasmaspheric hiss derived from Van Allen probes data and their effects on radiation belt electron dynamics. *Journal of Geophysical Research: Space Physics*, *120*, 3393–3405. https://doi.org/10.1002/2015JA021048

Ma, Q., Li, W., Thorne, R. M., Bortnik, J., Reeves, G. D., Kletzing, C. A., et al. (2016). Characteristic energy range of electron scattering due to plasmaspheric hiss. *Journal of Geophysical Research: Space Physics*, *121*(12), 11,737–11,749. https://doi.org/10.1002/2016JA023311

Malaspina, D. M., Jaynes, A. N., Boulé, C., Bortnik, J., Thaller, S. A., Ergun, R. E., et al. (2016). The distribution of Plasmaspheric hiss wave power with respect to Plasmapause location. *Geophysical Research Letters*, *43*, 7878–7886. https://doi.org/10.1002/2016GL069982

Meredith, N. P., Horne, R. B., Kersten, T., Li, W., Bortnik, J., Sicard, A., & Yearby, K. H. (2018). Global model of plasmaspheric hiss from multiple satellite observations. *Journal of Geophysical Research: Space Physics*, *123*, 4526–4541. https://doi.org/10.1029/2018JA025226

Meredith, N. P., Horne, R. M., Glauert, S. A., Baker, D. N., Kanekal, S. G., & Albert, J. M. (2009). Relativistic electron loss timescales in the slot region. *Journal of Geophysical Research*, *114*, A03222. https://doi.org/10.1029/2008JA013889

Meredith, N. P., Thorne, R. B., Horne, R. M., Summers, D., & Anderson, R. R. (2004). Substorm dependence of plasmaspheric hiss. *Journal of Geophysical Research*, *109*, A06209. https://doi.org/10.1029/2004JA010387

Mourenas, D., Artemyev, A. V., Ma, Q., Agapitov, O. V., & Li, W. (2016). Fast dropouts of multi-MeV electrons due to combined effects of EMIC and whistler mode waves. *Geophysical Research Letters*, *43*, 4155–4163. https://doi.org/10.1002/2016GL068921

Mourenas, D., Artemyev, A. V., Ripoll, J.-F., Agapitov, O. V., & Krasnoselskikh, V. V. (2012). Timescales for electron quasi-linear diffusion by parallel and oblique lower-band chorus waves. *Journal of Geophysical Research*, *117*, A06234. https://doi.org/10.1029/2012JA017717

Mourenas, D., Ma, Q., Artemyev, A. V., & Li, W. (2017). Scaling laws for the inner structure of the radiation belts. *Geophysical Research Letters*, *44*, 3009–3018. https://doi.org/10.1002/2017GL072987

Mourenas, D., & Ripoll, J. F. (2012). Analytical estimates of quasi-linear diffusion coefficients and electron lifetimes in the inner radiation belt. *Journal of Geophysical Research*, *117*, A01204. https://doi.org/10.1029/2011JA016985

Ni, B., Bortnik, J., Thorne, R. M., Ma, Q., & Chen, L. (2013). Resonant scattering and resultant pitch angle evolution of relativistic electrons by plasmaspheric hiss. *Journal of Geophysical Research: Space Physics*, *118*, 7740–7751. https://doi.org/10.1002/2013JA019260

O'Brien, T. P., & Moldwin, M. B. (2003). Empirical plasmapause models from magnetic indices. *Geophysical Research Letters*, *30*(4), 1152. https://doi.org/10.1029/2002GL016007

Orlova, K., Shprits, Y., & Spasojevic, M. (2016). New global loss model of energetic and relativistic electrons based on Van Allen probes measurements. *Journal of Geophysical Research: Space Physics*, *121*, 1308–1314. https://doi.org/10.1002/2015JA021878

Ozeke, L. G., Mann, I. R., Murphy, K. R., Degeling, A. W., Claudepierre, S. G., & Spence, H. E. (2018). Explaining the apparent impenetrable barrier to ultra-relativistic electrons in the outer Van Allen belt. *Nature Communications*, *9*(1), 1844. https://doi.org/10.1038/s41467-018-04162-3

Ozhogin, P., Tu, J., Song, P., & Reinisch, B. W. (2012). Field-aligned distribution of the plasmaspheric electron density: An empirical model derived from the IMAGE RPI measurements. *Journal of Geophysical Research*, *117*, A06225. https://doi.org/10.1029/2011JA017330

Pinto, V. A., Mourenas, D., Bortnik, J., Zhang, X.-J., Artemyev, A. V., Moya, P. S., & Lyons, L. R. (2019). Decay of ultrarelativistic remnant belt electrons through scattering by plasmaspheric his. *Journal of Geophysical Research: Space Physics*, *124*, 5222–5233. https://doi.org/10.1029/2019JA026509

Sheeley, B. W., Moldwin, M. B., Rassoul, H. K., & Anderson, R. R. (2001). An empirical plasmasphere and trough density model: CRRES observations. *Journal of Geophysical Research*, *106*(A11), 25,631–25,641. https://doi.org/10.1029/2000JA000286

Spasojevic, M., Shprits, Y. Y., & Orlova, K. (2015). Global empirical models of plasmaspheric hiss using Van Allen probes. *Journal of Geophysical Research, Space Physics*, *117*, 370–10,383. https://doi.org/10.1002/2015JA021803

Su, Z., Liu, N., Zheng, H., Wang, Y., & Wang, S. (2018a). Large-amplitude extremely low frequency hiss waves in plasmaspheric plumes. *Geophysical Research Letters*, *45*, 565–577. https://doi.org/10.1002/2017GL076754

Su, Z., Liu, N., Zheng, H., Wang, Y., & Wang, S. (2018b). Multipoint observations of nightside plasmaspheric hiss generated by substorm-injected electrons. *Geophysical Research Letters*, *45*, 10,921–10,932. https://doi.org/10.1029/2018GL079927

Summers, D., Ni, B., & Meredith, N. P. (2007). Timescales for radiation belt electron acceleration and loss due to resonant wave-particle interactions: 2. Evaluation for VLF chorus, ELF hiss, and electromagnetic ion cyclotron waves. *Journal of Geophysical Research*, *112*, A04207. https://doi.org/10.1029/2006JA011993

Thorne, R. M., Li, W., Ni, B., Ma, Q., Bortnik, J., Baker, D. N., et al. (2013). Evolution and slow decay of an unusual narrow ring of relativistic electrons near L ~ 3.2 following the September 2012 magnetic storm. *Geophysical Research Letters*, *40*, 3507–3511. https://doi.org/10.1002/grl.50627

Watt, C. E. J., Allison, H. J., Meredith, N. P., Thompson, R. L., Bentley, S. N., Rae, I. J., et al. (2019). Variability of Quasilinear diffusion coefficients for Plasmaspheric hiss. *Journal of Geophysical Research: Space Physics*, *124*, 8488–8506. https://doi.org/10.1029/2018JA026401

Yu, J., Li, L. Y., Cao, J. B., Chen, L., Wang, J., & Yang, J. (2017). Propagation characteristics of plasmaspheric hiss: Van Allen probe observations and global empirical models. *Journal of Geophysical Research: Space Physics*, *122*, 4156–4167. https://doi.org/10.1002/2016JA023372

Zhang, X.-J., Li, W., Thorne, R. M., Angelopoulos, V., Bortnik, J., Kletzing, C. A., et al. (2016). Statistical distribution of EMIC wave spectra: Observations from Van Allen probes. *Geophysical Research Letters*, *43*, 12,348–12,355. https://doi.org/10.1002/2016GL071158